ARL-TR-10263 ● JAN 2026

Optimization of Digital Image Correlation Patterning with Laser-Based Methods

by Glen W. Cockcroft, Michael T. Hurst, Braden L. Miller, Daniel O. Lewis, and Brady G. Butler

NOTICES

Disclaimers

ARL-TR-10263 ● JAN 2026

Optimization of Digital Image Correlation Patterning with Laser-Based Methods

Glen W. Cockcroft, Braden L. Miller, and Daniel O. Lewis
Texas A&M University, Department of Materials Science and Engineering

Michael T. Hurst
Texas A&M University, Bush Combat Development Complex

Brady G. Butler
DEVCOM Army Research Laboratory

REPORT DOCUMENTATION PAGE

1. REPORT DATE	2. REPORT TYPE	3. DATES COVERED	
		START DATE	END DATE
January 2026	Technical Report	27 May 2025	30 November 2025

4. TITLE AND SUBTITLE
Optimization of Digital Image Correlation Patterning with Laser-Based Methods

5a. CONTRACT NUMBER	5b. GRANT NUMBER	5c. PROGRAM ELEMENT NUMBER
W911NF-22-F-0032		
5d. PROJECT NUMBER	**5e. TASK NUMBER**	**5f. WORK UNIT NUMBER**

6. AUTHOR(S)
Glen W. Cockcroft, Michael T. Hurst, Braden L. Miller, Daniel O. Lewis, and Brady G. Butler

7. PERFORMING ORGANIZATION NAME(S) AND ADDRESS(ES)	8. PERFORMING ORGANIZATION REPORT NUMBER
DEVCOM Army Research Laboratory ATTN: FCDD-RLA-MF College Station, TX 77840	ARL-TR-10263

9. SPONSORING/MONITORING AGENCY NAME(S) AND ADDRESS(ES)	10. SPONSOR/MONITOR'S ACRONYM(S)	11. SPONSOR/MONITOR'S REPORT NUMBER(S)

12. DISTRIBUTION/AVAILABILITY STATEMENT
DISTRIBUTION STATEMENT A. Approved for public release: distribution unlimited.

13. SUPPLEMENTARY NOTES
ORCIDs: Glen W. Cockcroft, 0009-0005-5464-1115; Braden L. Miller, 0009-0004-0382-2699; Daniel O. Lewis, 0000-0002-3427-7265; Michael T. Hurst, 0000-0002-6138-2634; Brady G. Butler, 0000-0002-7677-9685

14. ABSTRACT
This study covers the creation and optimization of a method for digital image correlation (DIC) analysis on niobium and copper substrates using a 20-W fiber laser. Initially, speckle size, contrast, density, and stochasticity parameters were identified for determining speckle pattern quality. Python scripts were developed to collect image data based on these parameters to be accurately scored for comparison. Vector and bitmap image patterns were then generated using Python code using placement masks and Poisson disc sampling methods, respectively. The vector patterns were ablated with 40% power and on copper substrates for compression testing with 3D DIC strain mapping. The bitmap patterns were ablated on a niobium surface polished at 800 grit and coated with black acrylic paint using 90% power and 15 loop counts for compression testing with 2D DIC mapping. The resulting strain maps revealed patterns capable of performing accurate and detailed tracking even under extreme deformation. In addition, pattern scores were compared with negative and positive control patterns using the Python script, providing evidence for the developed speckle quality. Overall, the results revealed high-quality patterns that were easily replicable using simplified methods.

15. SUBJECT TERMS
digital image correlation, DIC, speckle pattern analysis, mechanical testing, compression, fiber laser, profilometer surface mapping, Sciences of Extreme Materials

16. SECURITY CLASSIFICATION OF:			17. LIMITATION OF ABSTRACT	18. NUMBER OF PAGES
a. REPORT	b. ABSTRACT	C. THIS PAGE		
UNCLASSIFIED	UNCLASSIFIED	UNCLASSIFIED	UU	25

19a. NAME OF RESPONSIBLE PERSON	19b. PHONE NUMBER *(Include area code)*
Brady G. Butler	(520) 691-5844

STANDARD FORM 298 (REV. 5/2020)
Prescribed by ANSI Std. Z39.18

Contents

List of Figures

List of Tables

1. Introduction

Digital image correlation (DIC) is a computational strain measurement technique that has gained significant popularity over the past decades (Figure 1). Commonly used tools (i.e., strain gauges and extensometers) along with more advanced methods (i.e., the grid method) have all in some way fallen short of the high versatility and analytical power DIC brings for minimal cost of time and effort. Using a speckle pattern applied to the sample's surface to track the grayscale variation across a specified grid, DIC allows for accurate local strain measurements across the surface of a sample, even for highly complex geometries.

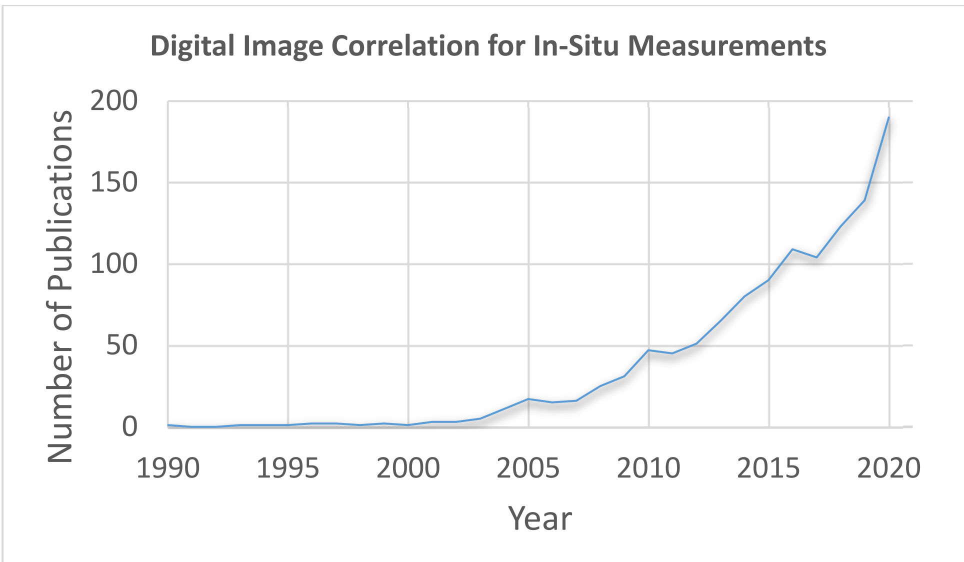

Figure 1. Publications of DIC for in-situ strain measurements (modified from Cunha et al. 2021).

DIC provides unparalleled access to surface strain fields in two and three dimensions, but the reliability of these measurements is constrained by the speckle pattern, which must adhere to carefully defined quality parameters. While many exist, the right method for speckle pattern development is highly ambiguous and has undergone much research over time. Several different methods—from spray paint to photolithography—have been used to generate an ideal pattern. While all have advantages and disadvantages, laser ablation is one method that has been gaining interest. Using a laser to ablate a speckle pattern allows for high precision at fast processing speeds. Despite this, such a method seems to have undergone minimal study. Therefore, it became the goal of this research experience to develop a simple and versatile laser-ablation method for DIC patterning. In the end, two different patterns (one tailored for 2D DIC and the other for 3D) were created to score in comparison to a negative and positive control.

2. Methods

Given there is no universal DIC speckle patterns rating system, the first task of this research project was to determine a viable scoring method for pattern quality. This was done by outlining four important characteristics of speckle patterns found across the reviewed literature (Pan et al. 2009; Schreier et al. 2009; Dong and Pan 2017; Szalai and Dogossy 2021): contrast, density, size, and stochasticity. To quantify these characteristics, they were divided into several parameters, which are depicted in Figures 2–5 using the Sample 17 pattern from the DIC Challenge research experiment, due to its ideal qualities (Reu et al. 2018). More on this pattern can be found in Section 4.

2.1 Contrast

The parameters chosen to measure the contrast quality of speckle patterns were Michelson contrast and contrast variance. Michelson contrast indicated the breadth of the grayscale intensity, while contrast variance determined the distribution. Both values would, in an ideal scenario, have a value of one, indicating a speckle pattern with maximum contrast between speckles and background.

One of the first steps taken in scoring a speckle pattern was converting the image of interest into a binary format where the speckles were all white and the background all black, or vice versa. This was done by calculating a threshold value to divide the image into either black or white pixels. As shown in Figure 2, two thresholds were calculated: Otsu and local. The Otsu threshold was able to determine the ideal dividing line based on the entirety of pixel intensity data. On the other hand, the local threshold was able to determine the ideal dividing line when ignoring poor lighting distribution. Hence, a binary image generated with the local threshold was used for the size metrics, while the Otsu threshold was used to generate a binary image for the rest. This ensured greater accuracy when calculating the speckle pattern's metrics and overall score.

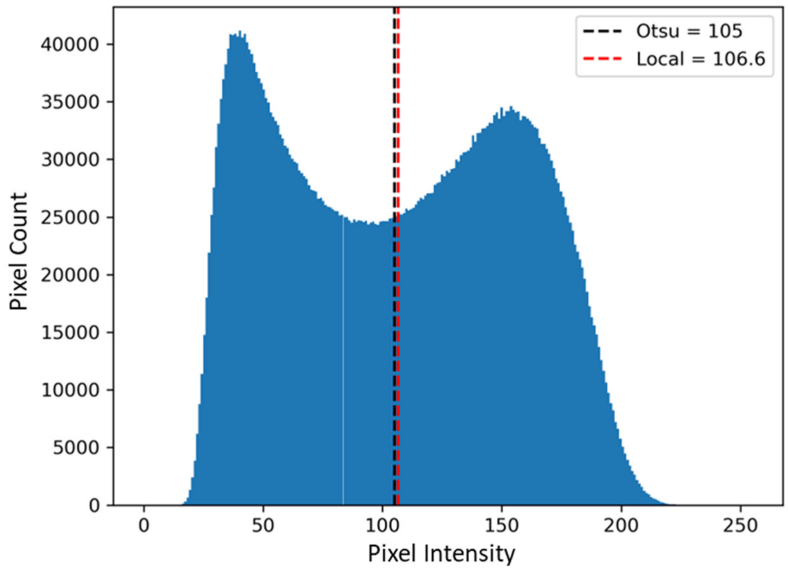

Figure 2. Pixel intensity histogram for iDIC Sample 17 (Reu et al. 2018).

2.2 Density

Speckle pattern density was simply calculated by determining the area fraction, or percentage of area covered by the speckles alone. It is generally recommended that the speckled area comprise 50% coverage to ensure no empty or overfilled spaces (Figure 3).

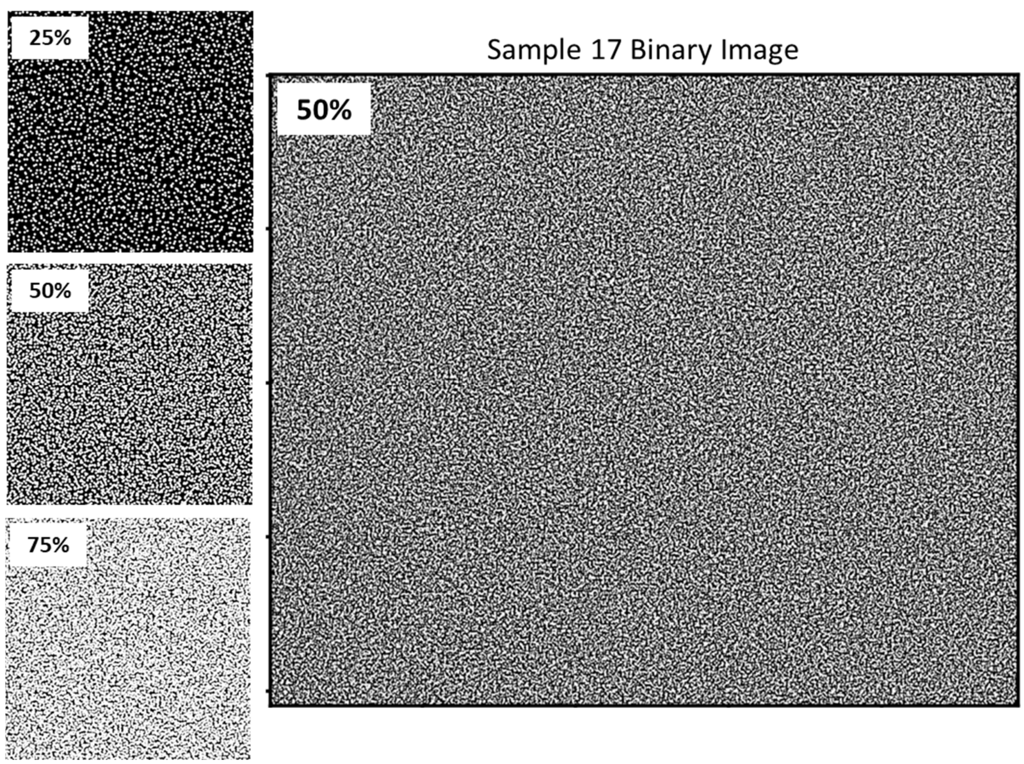

Figure 3. Binary image examples and iDIC Sample 17 (Reu et al. 2018) at 50% coverage.

2.3 Size

The size of a speckle depends on the imaging conditions used in DIC; higher-resolution cameras can utilize smaller speckles and achieve better strain resolution in practice. An ideal speckle size is generally on the order of 5 pixels in diameter (Dong and Pan 2017; Szalai and Dogossy 2021). The size and shape of speckle patterns can be measured several ways. In this study, speckle size metrics were limited to mean local thickness, speckle size variation, and eccentricity. The local thickness measures the largest inscribed circle diameter at each pixel, which can be averaged to estimate the size while disregarding any overlap that may occur between speckles. The local thickness and speckle area measurements of an optimized pattern are shown in Figure 4. Speckle size variation quantified the range in speckle size. An ideal speckle size variation value would be zero as it implies there is no variation. Finally, eccentricity indicated the circularity of the speckles, with a value of zero being the most circular and therefore the ideal value. This metric also helped quantify the amount of speckle overlap, as overlapping speckles were generally grouped together as a singular one, resulting in a poorer eccentricity score.

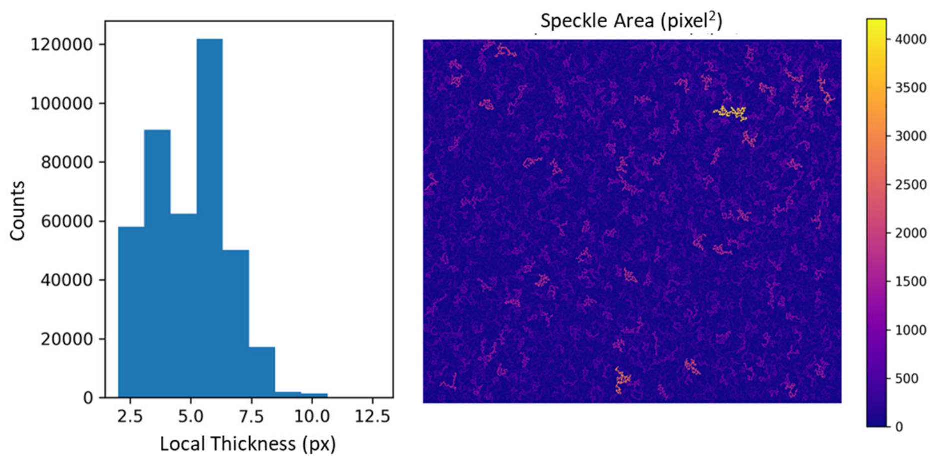

Figure 4. Thickness histogram and speckle area map of iDIC Sample 17 (Reu et al. 2018).

2.4 Stochasticity

Stochasticity, or the randomness of the speckle pattern, was addressed through grid uniformity and periodicity. Grid uniformity measured the change in brightness across the entire pattern by splitting it into a 10 × 10 grid and calculating the standard deviation between the background area fractions of each section. This displayed any serious variations in lighting across the speckle pattern image. Hence, a grid uniformity of zero was most desirable. Periodicity measured repetitive spacing between speckles. This was done by plotting the radial autocorrelation profile of the pattern and counting the resulting number of peaks. More peaks meant there was a somewhat predictable relation between the speckles. Ideally, a pattern should have zero peaks (Figure 5).

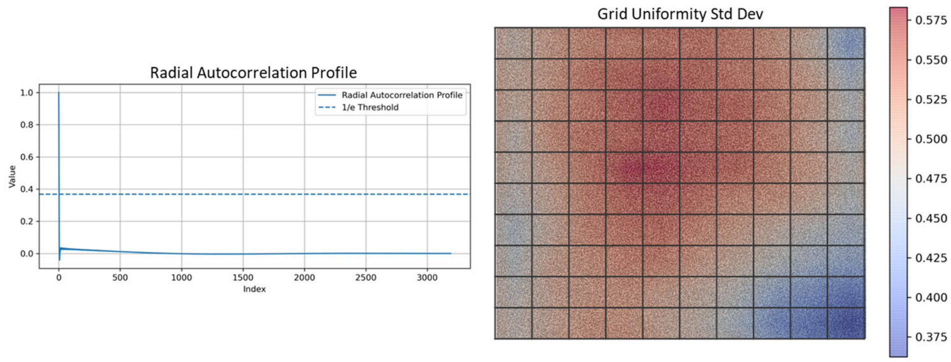

Figure 5. Periodicity and grid uniformity of iDIC Sample 17.

2.5 Overall Score

Each previously described metric was determined by running any pattern image through a Python script. These values were then compared to ideal values with specified tolerances to accurately score the patterns being analyzed (Table 1).

Table 1. Selected values for score comparison.

Metric	Reference	Tolerance
Mean local thickness (PX)	5	5
Speckle size variation	0	2
Eccentricity	0	2
Area fraction (%)	50	50
Michelson contrast	1	1
Contrast variance	1	2
Grid uniformity (%)	0	50
Periodicity	0	50

The actual metric data was then combined with reference and tolerance values via Equation 1 to produce an overall score for each pattern.

$$Overall\ Score = mean\left(100 \times \left(1 - \frac{actual - reference}{tolerance}\right)\right) \quad (1)$$

2.6 Laser Marking

Now that the patterns could be adequately quantified and compared for overall quality assessment, the actual development of a pattern via laser-based methods was in order. For speckle ablation we used the LaserGear BOQX laser with specifications as shown in Table 2. To create a simple pattern using this fiber laser, two types of digital patterns were generated using different Python scripts and ablated onto a surface with a black coating.

Table 2. Fiber laser system parameters.

LaserGear BOQX system	
Laser type	MOPA Ytterbium fiber
Wavelength	1062 ± 3 nm
Wattage rating	20 W
Frequency range	1–400 kHz
Pulse duration	200 ns
Operative ambient air temp	0–40 °C
Cooling type	Forced air
Focus beam	Class II
Laser spot size	35 µm (163 lens)
Max part size	12-inches W × 9-inches L × 5.75-inches H

The first pattern was developed by generating random coordinates and placing speckles at each as long as they were not touching. Any speckle radius could be used as long as it was greater than 1 pixel. The pattern could then be imported into the laser software as a vector file, so the laser could trace the inner contour of each speckle. This allowed for extremely precise speckles across a variety of sizes. The pattern was ablated at 40% power since a permanent black marker was used as the background coating for vector files due to its easy application and reproducibility (Figure 6).

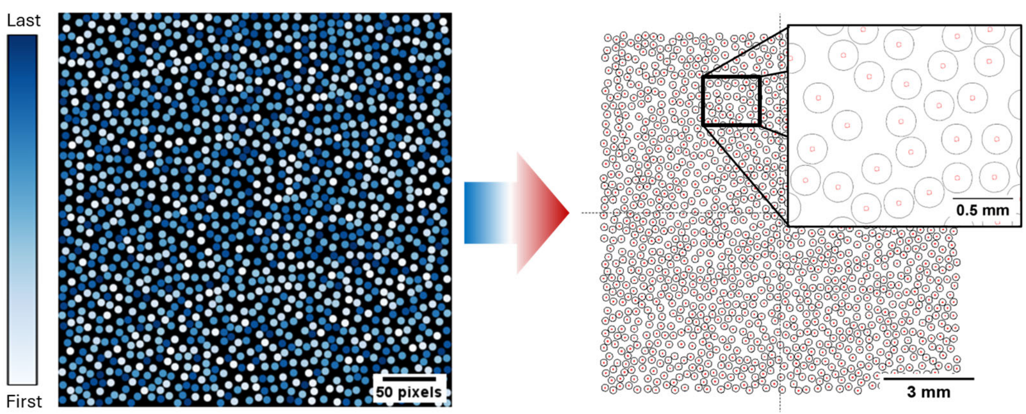

Figure 6. Digital generation (in blue) to physical ablation (in red) for vector patterns.

One issue, though, was the vector-generated patterns could not be decreased to the absolute minimum speckled size possible (i.e., the smallest effective laser beam diameter of ~35 µm). This was important as 2D DIC had a higher resolution and therefore required a smaller speckle size to achieve the ideal mean local thickness of 5 pixels. Hence, a new Python script using Poisson disc sampling with Bridson's algorithm was developed to generate single-pixel spots with greater stochasticity and less computational power consumption. This was possible since Poisson disc sampling generates speckles within a certain distance from each other, branching randomly outward rather than placing speckles randomly across the entire surface (Bridson 2007). These were then imported into the laser software as bitmap files; thereby, causing the laser to ablate once per pixel given a specified dwell duration. This resulted in an extremely fine pattern with approximately 35-μm-diameter speckles. Given the sensitivity of the small speckles to surface scratches, an 800-grit polish was applied, and acrylic paint was selected over a permanent marker as the background coating to ensure greater uniformity. The patterns had to be ablated at 90% power for 15 loop counts, due to the thicker coating (Figure 7).

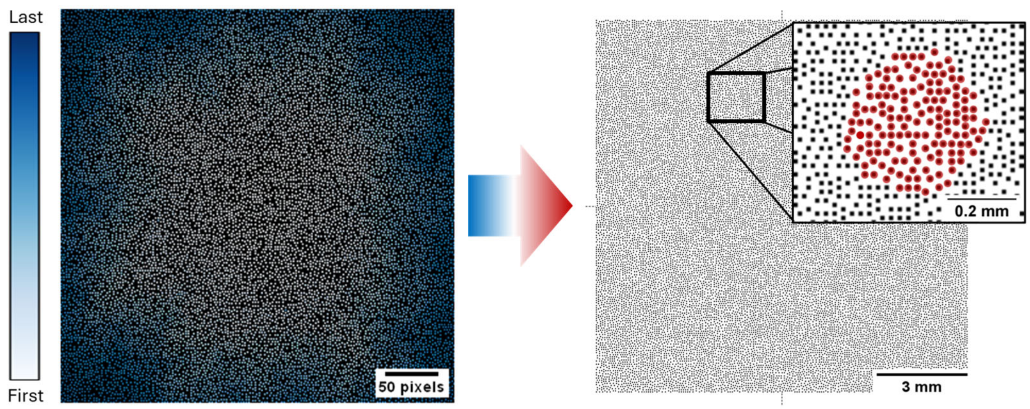

Figure 7. Digital generation (in blue) to physical ablation (in red) for bitmap patterns.

3. Results

To ensure the coating methods were the appropriate thicknesses, height maps at high magnifications were taken of the vector and bitmap ablated speckles using a Keyence VK-X1000 profilometer (Figure 8). The total ablated depth to remove the permanent marker coating was found to be roughly 8 μm and the acrylic paint coating was found to be roughly 15 μm. Since these were well within an acceptable range for DIC coating thickness, the final prints were mechanically tested in compression at a crosshead displacement rate of 0.010 mm/s. The stereoscopic vector pattern images were analyzed with 3D DIC, while 2D DIC was used for the bitmap patterns.

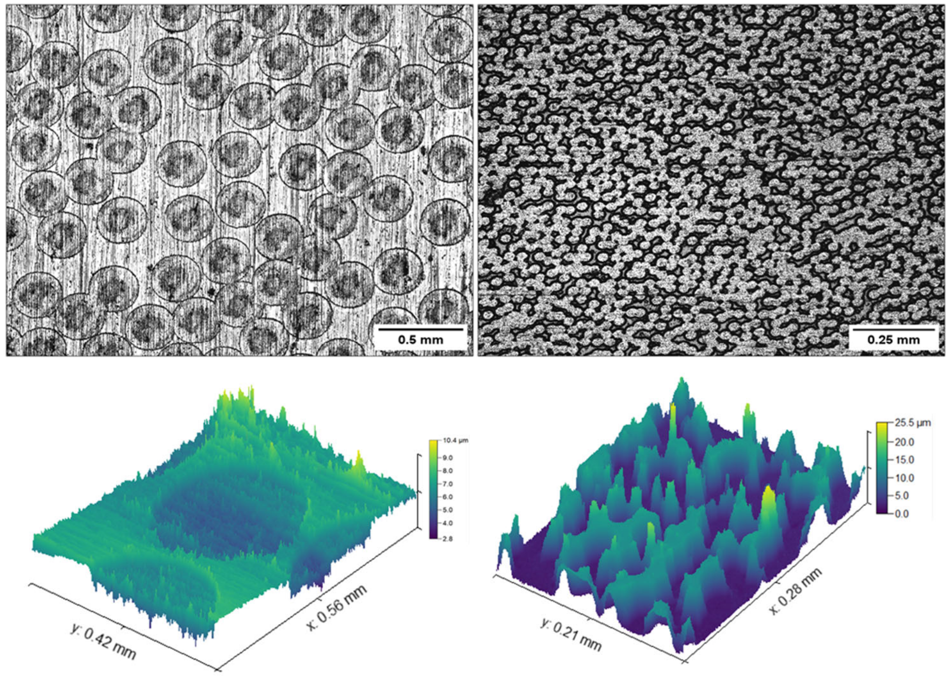

Figure 8. Keyence height maps of vector (left) and bitmap (right) patterns.

For the vector patterns tested via 3D DIC analysis, one copper and one niobium sample were used. Since the resolution for the 3D setup was roughly 50 µm/pixel, the spot size was set to 250 µm to achieve the ideal 5-pixel speckle diameter. Von Mises strain maps were generated using VIC-3D software with a subset size of 17 and a step size of 4. Based on the subset size, the spatial resolution for each step was 850 µm. As shown in Figure 9, DIC Von Mises strain and digital extensometer strain data were plotted with compression machine data as stress versus strain curves.

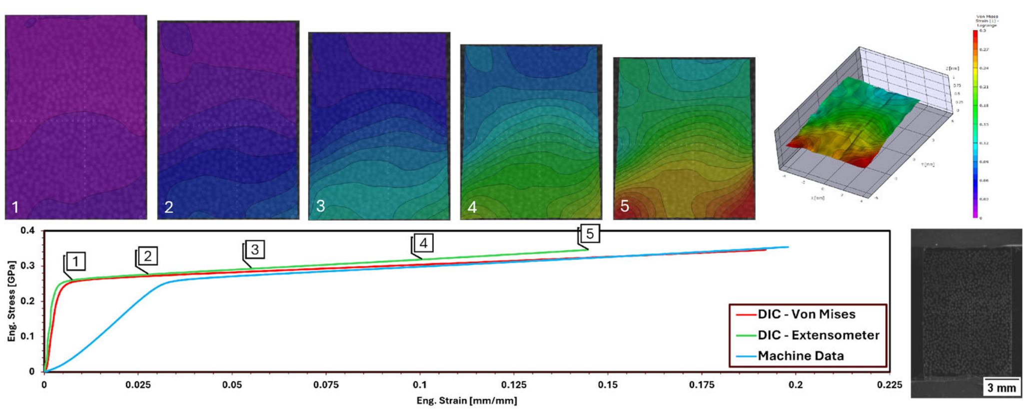

Figure 9. VIC-3D analysis of copper compression using vector pattern.

For the bitmap patterns tested via 2D DIC analysis, two copper and two niobium samples were used. The 2D setup had a resolution of roughly 7 µm/pixel; thus, creating the ideal scenario for a spot size of 35 µm as generated in the bitmap patterns. Von Mises strain maps were generated using VIC-2D software with a subset size of 25 and a step size of 6. Based on the subset size, the resulting spatial resolution was 175 µm. Figure 10 shows the DIC Von Mises strain and digital extensometer strain data plotted with compression machine data as stress versus strain curves.

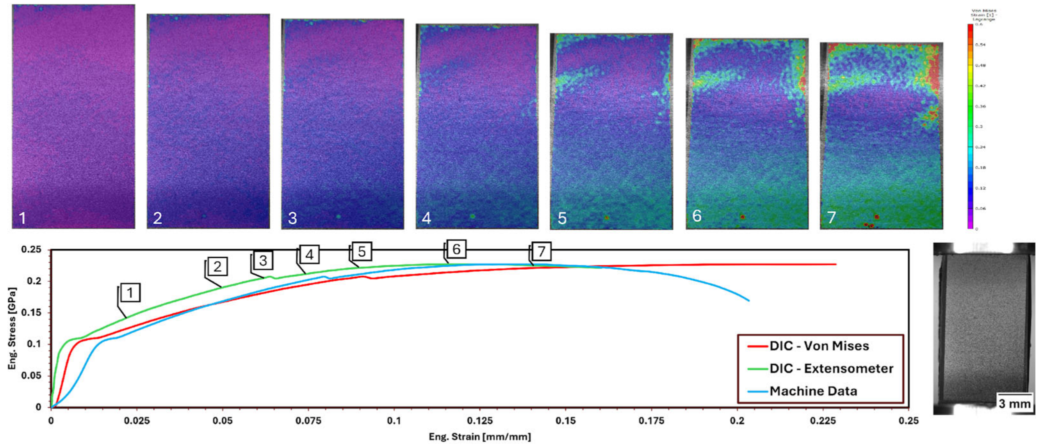

Figure 10. VIC-2D analysis of niobium compression using bitmap pattern.

4. Discussion

The stress versus strain curves, shown in Figures 9 and 10, exhibit a steeper initial yield in the DIC data compared with the machine data. This difference arises because the machine data includes the elastic response of the entire compression setup in addition to the sample strain. One of the strengths of DIC analysis is its ability to isolate rotation, translation, and deformation in the sample itself while excluding compliance effects from the surrounding apparatus. The similarity among the DIC and machine curves, even with this distinction, indicates that the speckle patterns were accurately tracking the sample's strain.

In the 2D stress versus strain curve, the data also reveal sample slippage during deformation, visible as a sudden drop in stress near the midpoint of the curve. The fact that this event is captured in both the DIC and machine data confirms that DIC analysis is faithfully recording strain across the sample surface without introducing additional bias.

To assess pattern quality, the final vector and bitmap patterns were compared against a negative and a positive control, as shown in Figure 11. The negative control was a spray-painted pattern from past U.S. Army Combat Capabilities Development Command Army Research Laboratory experiments (Moody et al. 2020). Spray-painting is simple and widely used but often produces inconsistent and imprecise results. The positive control was Sample 17 from the DIC Challenge study (Reu et al. 2018), a laser-printed peel-and-stick label that represents a near-ideal speckle pattern, though unsuitable for actual deformation testing.

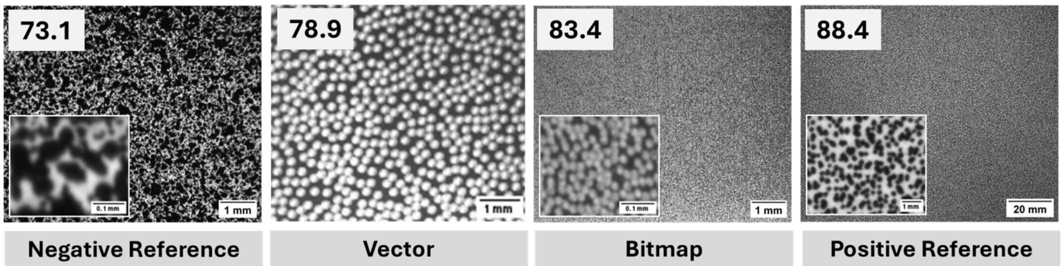

Figure 11. Final score comparison using negative and positive controls.

The laser-ablated patterns produced in this study achieved noticeably higher scores (~5–10 points greater) than the spray-painted standard. The bitmap pattern scored only five points lower than the positive control, which is notable given that the latter was fabricated under ideal conditions and not tested under load. In addition, the bitmap speckle size (~35 μm) was much finer than that of Sample 17, further underscoring the precision of the approach. These findings demonstrate that the laser-ablated patterns met the project's goal of producing high-quality reproducible speckle fields.

To validate the scoring results, uncertainty estimates were obtained directly from the VIC-2D and VIC-3D software using a constant subset size of 25 pixels and an imposed noise level of 8. VIC reports the 1 standard deviation displacement uncertainty (i.e., in units of pixels), which reflects the local curvature of the correlation surface and therefore the confidence in the subset match. Although the software does not explicitly implement the closed-form expression proposed by Reu et al. (2009), the reported sigma values are governed by the same underlying factors: image noise and the local intensity gradients within each subset. For context, Reu's 1D, theoretical form for the Cramér–Rao lower bound is shown in Equation 2.

$$\sigma\ (pixels) = \sqrt{\frac{var \times \sum_{i=1}^{n}[\nabla T(x_i)]^2}{2}} \tag{2}$$

This illustrates the dependence of DIC uncertainty (σ), on both the noise variance (var) and the summed intensity gradient ($\nabla\, T(x_i)$).

Representative uncertainty values from VIC are provided in Figure 12, and summary statistics are listed in Table 3. For most patterns, the measured uncertainty was consistent with the calculated scoring results, supporting the validity of the bitmap-based quality metric. The vector pattern, however, exhibited lower uncertainty than expected based on its score. This discrepancy appears to result from image acquisition rather than the patterning method; the captured intensity range did not span the full grayscale (0 to 255), suppressing the measured contrast and lowering the calculated score. Because the scoring algorithm weights contrast strongly, the vector pattern's score was disproportionately reduced.

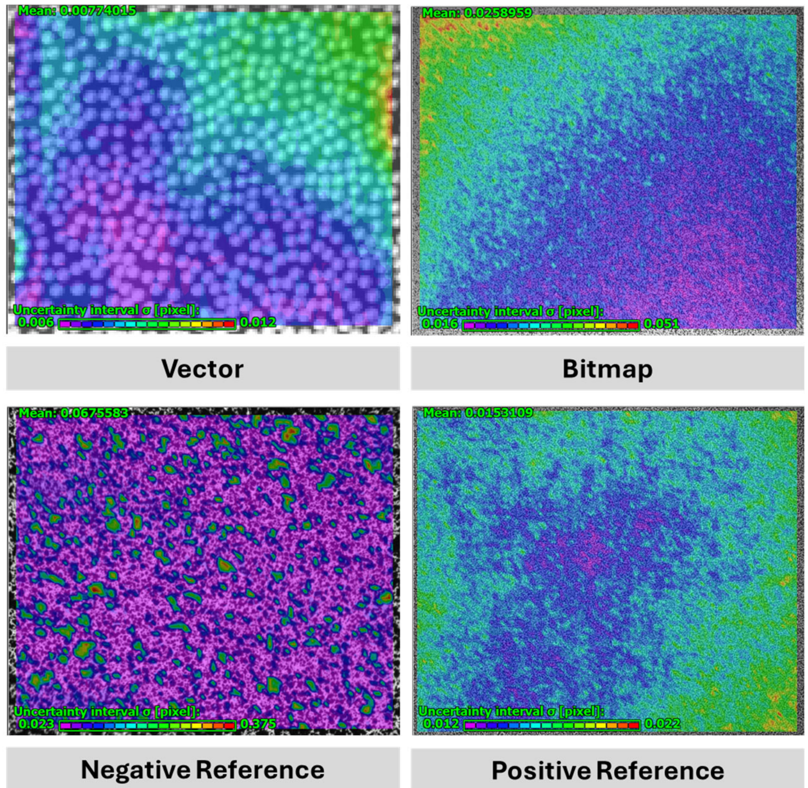

Figure 12. **VIC software uncertainty interval comparison of patterns.**

Table 3. **Uncertainty interval for various patterning techniques.**

Uncertainty interval (pixel)	Min.	Max.	Mean
Vector	0.006	0.012	0.00774015
Bitmap	0.016	0.051	0.0258959
Negative reference	0.023	0.375	0.0675583
Positive control	0.012	0.022	0.0153109

It is also important to distinguish the intended operating regimes of the two patterning approaches. The 3D vector patterns were optimized for a lower-resolution imaging system with a laser spot size near 250 µm, while the 2D bitmap patterns approached the resolution limit of the laser system at roughly 35 µm. Both patterning strategies can be tuned to different imaging systems by selecting appropriate speckle sizes. Improvements in camera calibration and lighting control, particularly through high–dynamic-range acquisition, would further reduce uncertainty in future work. Additional comparisons with DIC Challenge patterns (Reu et al. 2018) are included in the Appendix.

5. Conclusion

This study established a laser-based DIC patterning workflow supported by a quantitative scoring system for speckle quality. Vector and bitmap patterns were designed for 3D and 2D DIC, respectively, and validated through full-field compression testing on niobium and copper samples. Both approaches produced high-fidelity strain maps and achieved scores comparable to or exceeding established benchmarks, such as the DIC Challenge.

The scoring framework provides an unbiased and reproducible means of assessing speckle quality, incorporating metrics for contrast, size, density, and stochasticity. Its modular design allows straightforward adaptation to different imaging conditions, higher-resolution systems, and other patterning methods. The combined outcomes of this work advance the practical application and scientific rigor of DIC patterning and provide a foundation for continued refinement and broader standardization in the field.

6. References

Bridson R. Fast Poisson disk sampling in arbitrary dimensions. In: ACM SIGGRAPH 2007 sketches. ACM; 2007; p. 22. https://doi.org/10.1145/1278780.1278807

Cunha FG, Santos TG, Xavier J. In situ monitoring of additive manufacturing using digital image correlation: a review. Materials. 2021;14(6):1511. https://doi.org/10.3390/ma14061511

Dong YL, Pan B. A review of speckle pattern fabrication and assessment for digital image correlation. Exp Mech. 2017;57(8):1161–1181. https://doi.org/10.1007/s11340-017-0283-1

Moody LC et al. Cross-sectional area measurement by optical and electrical resistance methods for subscale mechanical testing of near-net-shape titanium components. Int J Refract Metals Hard Mater. 2020;92:105265. https://doi.org/10.1016/j.ijrmhm.2020.105265

Pan B, Qian K, Xie H, Asundi A. Two-dimensional digital image correlation for in-plane displacement and strain measurement: a review. Meas Sci Technol. 2009;20(6):062001. https://doi.org/10.1088/0957-0233/20/6/062001

Reu PL et al. DIC Challenge: developing images and guidelines for evaluating accuracy and resolution of 2D analyses. Exp Mech. 2018;58(7):1067–1099. https://doi.org/10.1007/s11340-017-0349-0

Reu PL, Sutton M, Wang Y, Miller TJ. Uncertainty quantification for digital image correlation. Sandia National Laboratories (US); 2009. https://www.osti.gov/servlets/purl/1142312

Schreier H, Orteu J-J, Sutton MA. Image correlation for shape, motion and deformation measurements. Springer (US); 2009. https://link.springer.com/10.1007/978-0-387-78747-3

Szalai S, Dogossy G. Speckle pattern optimization for DIC technologies. Acta Technica Jaurinensis. 2021;14(3):228–243. https://doi.org/10.14513/actatechjaur.00573

Appendix. Pattern Scoring Results and Code

A-1. Pattern Score Comparison

A comparison of speckle pattern scores from the current study alongside patterns from the Digital Image Correlation (DIC) Challenge and prior internal experiments at the U.S. Army Combat Capabilities Development Command (DEVCOM) Army Research Laboratory (ARL) are shown in Figure A-1. The laser-ablated vector and bitmap patterns developed in this project achieved significantly higher scores than the spray-painted ARL control and approached the benchmark performance of DIC Challenge Sample 17, a near-ideal peel-and-stick pattern.

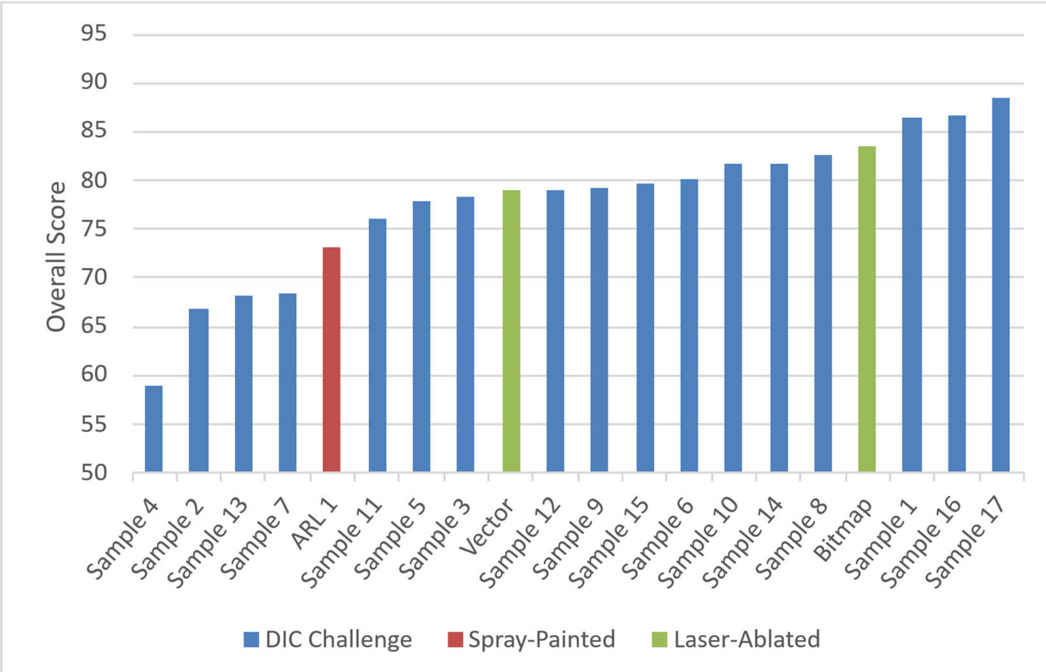

Figure A-1. Score comparison of DIC Challenge, ARL spray-painted, and laser-ablated patterns.[1,2]

These results further validate the robustness of the scoring framework and demonstrate the capability of laser ablation to generate patterns that are not only visually high quality, but also quantitatively comparable to community benchmarks. Notably, while the DIC Challenge patterns were printed and not subjected to deformation, the laser-ablated patterns shown here were successfully

[1] Reu PL et al. DIC challenge: developing images and guidelines for evaluating accuracy and resolution of 2D analyses. Exp Mech. 2018;58(7):1067–1099. https://doi.org/10.1007/s11340-017-0349-0

[2] Moody LC et al. Cross-sectional area measurement by optical and electrical resistance methods for subscale mechanical testing of near-net-shape titanium components. Int J Refract Metals Hard Mater. 2020;92:105265. https://doi.org/10.1016/j.ijrmhm.2020.105265

used in both 2D and 3D DIC during mechanical testing, making their performance even more meaningful in a practical context.

A-2. Open-Source Code for Pattern Generation and Scoring

All Python scripts developed during this project have been made publicly available to support reproducibility, further development, and broader application in the DIC research community. The code base consists of two pattern generation scripts and one pattern scoring script, each designed to address complementary aspects of DIC preparation and evaluation.

The first script serves as a vector pattern generator intended primarily for 3D DIC applications. It creates non-overlapping circular speckles by means of a randomized placement algorithm that ensures uniform coverage without overlap. The resulting patterns are exported as high-resolution TIFF images that can be readily imported into laser-marking software. Because these patterns are designed for systems with lower camera resolution and larger fields of view, they are well suited for 3D setups that require relatively large speckles. In this study the effective spot size was on the order of 250 µm.

The second script is a bitmap pattern generator optimized for 2D DIC. It uses Bridson's Poisson disk sampling algorithm to produce high-density randomized speckle fields. The generated features are represented as single pixels in binary TIFF images, which correspond directly to laser pulses when ablated. This approach makes it possible to generate patterns at the resolution limit of the laser marking system, approximately 35 µm in this study. The output files include metadata in their file names, which facilitates traceability and organization of experiments.

The third script provides a pattern scoring framework that evaluates speckle quality using a set of established metrics. It calculates contrast using Michelson contrast and variance; measures speckle density through area coverage; evaluates size using mean local thickness, variation, and eccentricity; and assesses stochasticity using grid uniformity and radial periodicity. Together, these metrics yield a weighted quality score for each pattern. In addition to numerical scoring, the script generates diagnostic outputs that aid interpretation. These include grayscale histograms with thresholding lines, autocorrelation, and correlation length profiles; fast Fourier transform log power spectra, entropy, and gradient magnitude maps; and heat maps of speckle area and eccentricity. The program also produces Microsoft Excel summary tables for each image and compiles combined reports when multiple patterns are analyzed. This combination of quantitative scoring and visual diagnostics makes the script a flexible tool for evaluating speckle quality and identifying avenues for further optimization.[*]

[*] All scripts are available at Python code used for 2D and 3D pattern generation and scoring (https://data.mendeley.com/datasets/v3cs9mgmr2/1). Each file includes documentation and example workflows to support adaptation for different substrates, imaging systems, or fabrication methods.

List of Symbols, Abbreviations, and Acronyms

1/2/3D	One-/Two-/Three-Dimensional
ARL	Army Research Laboratory
DEVCOM	U.S. Army Combat Capabilities Development Command
DIC	Digital Image Correlation
VIC	Virtual Image Correlation

1 (PDF)	DEFENSE TECHNICAL INFORMATION CTR DTIC OCA
1 (PDF)	DEVCOM ARL FCDD RLB CI TECH LIB